Available online at www.sciencedirect.com
SCIENCE DIRECT
Journal of Catalysis 226 (2004) 363–371
JOURNAL OF CATALYSIS
www.elsevier.com/locate/jcat

Co-containing polyoxometalate-based heterogeneous catalysts for the selective aerobic oxidation of aldehydes under ambient conditions

O.A. Kholdeeva [a,*], M.P. Vanina [a], M.N. Timofeeva [a], R.I. Maksimovskaya [a], T.A. Trubitsina [a], M.S. Melgunov [a], E.B. Burgina [a], J. Mrowiec-Bialon [b], A.B. Jarzebski [b], C.L. Hill [c,*]

[a] *Boreskov Institute of Catalysis, Pr. Ac. Lavrentieva 5, Novosibirsk 630090, Russia*
[b] *Polish Academy of Sciences, Institute of Chemical Engineering, 44-100 Gliwice, Baltycka 5, Poland*
[c] *Department of Chemistry, Emory University, 1515 Dickey Dr., Atlanta, GA 30322, USA*

Received 22 March 2004; revised 26 May 2004; accepted 29 May 2004

Available online 8 July 2004

Abstract

Tetra-*n*-butylammonium (TBA) salts of the cobalt-monosubstituted Keggin polyoxometalate (Co-POM), $TBA_4HPW_{11}CoO_{39}$ (**I**) and $TBA_5PW_{11}CoO_{39}$ (**II**), have been prepared and characterized by using elemental analysis, potentiometric titration, IR, UV–vis, ^{31}P NMR, and cyclic voltammetry. Different modes of heterogenization of the Co-POM, including anchoring to both NH_2- and NH_3^+-modified mesoporous silica surfaces and sol–gel synthesis, have been performed. The resulting solid catalysts were characterized by N_2-adsorption measurements, elemental analysis, DR-UV–vis, and FT-IR spectroscopy. The activity of the solid Co-POM materials to catalyze aerobic oxidation of two representative aldehydes, isobutyraldehyde (IBA) in MeCN and formaldehyde in H_2O under mild conditions (20–40 °C, 1 atm of air), was assessed and compared with the catalytic activity of the corresponding homogeneous Co-POMs. An emphasis has been placed on leaching tests and catalyst recycling. The effect of protonation of the amine-modified silica surface or the Co-POM on the loading, stability, and activity of the Co-POM solid catalyst was evaluated.

Keywords: Aldehyde; Aerobic oxidation; Cobalt; Supported polyoxometalates

1. Introduction

Aldehydes are important intermediates in synthetic chemistry as well as a significant pollutant in the human environment [1–3]. The development of heterogeneous catalysts for the aerobic oxidation of organic compounds is a challenging goal [4–9]. Transition-metal-substituted polyoxometalates (M-POMs for short) have attracted much attention as oxidation catalysts because of their unique ensemble of properties, including metal oxide-like structure, thermal and hydrolytic stability, tunable acidities and redox potentials, and alterable solubilities in various media, etc. [10–16]. Moreover, they can be supported on fabrics and porous materials [17–22]. It has been established that cobalt compounds, including Co-POMs, are among the best catalysts for homogeneous aerobic aldehyde oxidation and cooxidation of alkenes with aldehydes [1,23–25]. The superior activity of cobalt in these oxidations derives from its ability to initiate the radical chain process via interaction with the aldehyde molecule and from its participation in chain branching via interaction with the peroxy acid intermediate [26]. Several studies have addressed the preparation of solid Co-containing materials and their activity for aerobic aldehyde or alkene–aldehyde oxidations [19,20,22,25,27,28]. Co-POMs have been deposited on cotton cloth [19] and silica [20] and datively bonded to NH_2-modified silica surfaces [22]. Unfortunately, few of these efforts dealt with the issue of cobalt leaching under the reaction conditions or reported catalyst activity after recycling, both factors crucial for heterogeneous liquid-phase oxidation catalysts [4–6,9]. Here we report the preparation and characterization of different solid catalysts containing the cobalt-monosubstituted Keggin heteropolyanion, $[PW_{11}CoO_{39}]^{5-}$. Immobilization on both amine-modified mesoporous silica surface (NH_2–

* Corresponding author. Fax: +7 3832 343056.
E-mail addresses: khold@catalysis.nsk.su (O.A. Kholdeeva), chill@emory.edu (C.L. Hill).

0021-9517/$ – see front matter
doi:10.1016/j.jcat.2004.05.032

silica) and incorporation into silica during sol–gel synthesis have been studied. The catalytic activities of the solid Co-POM materials in the aerobic oxidation of isobutyraldehyde (IBA) in MeCN and formaldehyde in H_2O under mild conditions have been examined and the activities of these materials compared with catalytic activity of the corresponding homogeneous Co-POMs (the TBA- and Na-salts, respectively). The effect of protonation of the amine-modified silica surface or the Co-POM on the loading, activity, and stability of the Co-POM solid catalyst is discussed. The frequently success-limiting issues of catalyst leaching and catalyst reusability are addressed.

2. Experimental

2.1. Materials and catalysts

Acetonitrile (Fluka) was dried and stored over activated 3 Å molecular sieves. Isobutyraldehyde was purchased from Fluka and distilled prior to every experiment. Formaldehyde solutions were prepared by diluting 35.5% formalin, containing 2–4% of MeOH, with water. Preparations and purification of sodium and tetra-*n*-butylammonium salts of $[PW_{11}CoO_{39}]^{5-}$ were adapted from literature methods [22,24,29,30]. $TBA_4HPW_{11}CoO_{39}$ (**I**) and $TBA_5PW_{11}CoO_{39}$ (**II**) were prepared by metathesis of $Na_5PW_{11}CoO_{39}$ (**III**) with TBABr in water at pH 2.7 and 5, respectively. The purity of the compounds was checked by elemental analyses, IR, ^{31}P NMR, and cyclic voltammetry. The number of protons in the Co-POMs was determined by potentiometric titration with methanolic TBAOH (Aldrich).

2.1.1. $TBA_4HPW_{11}CoO_{39}$ (*I*)

The number of TBA cations, determined by ignition at 600 °C, was ca. 4.0 per one P atom. IR (1200–400 cm^{-1}, KBr, cm^{-1}): 1061, 956, 888, 818, 720. ^{31}P NMR (δ) (0.05 M in dry MeCN at 20 °C): 279 ppm ($\Delta\nu_{1/2} = 3700$ Hz). Potentiometric titration of **I** (0.05 mmol) in MeCN (5 mL) with 1 M methanolic TBAOH shows a sharp breakpoint at 1 eq of OH^- indicating a $[H^+]/[\mathbf{I}]$ ratio of 1.0. Elemental analysis (found/calc): W 54/55, Co 1.5/1.6.

2.1.2. $TBA_5PW_{11}CoO_{39}$ (*II*)

The number of TBA cations, determined by ignition, was ca. 5.0 per one P atom. IR (1200–400 cm^{-1}, KBr, cm^{-1}): 1061, 956, 888, 818, 752, 720. ^{31}P NMR (δ) (0.05 M in dry MeCN at 20 °C): 335 ppm ($\Delta\nu_{1/2} = 1500$ Hz). Potentiometric titration of **II** (0.05 mmol) in MeCN (5 mL) with 1 M methanolic TBAOH revealed no acid protons. Elemental analysis (found/calc): W 52/51, Co 1.5/1.5.

2.1.3. NH_2-functionalized mesoporous xerogel (NH_2–X)

This material was prepared using 10 mol% of *N*-[3-(trimethoxysilyl)propyl]ethylenediamine $(CH_3O)_3Si(CH_2)_3NHCH_2CH_2NH_2$ and ethyl silicate 40 as silica precursors by a procedure similar to that described in the literature [31]. The molar ratio of reagents was as follows: Si:H_2O:EtOH:NH_3 = 1:3:9:0.008. Typically, samples were prepared by mixing two solutions, the first one composed of 1/2 of the total amount of EtOH and the silica precursors, and the second one composed of 1/2 of the total amount of EtOH, water, and ammonia. After gelation and aging for 7 days at room temperature, the product materials were dried at 50 °C (4 days) and then 100 °C (5 h). The resulting NH_2–xerogel contained 1.23 mmol of NH_2 per 1 g of SiO_2.

2.1.4. The supported Co-POMs (samples *1*–*4*)

Samples **1** and **2** were prepared by dissolving 157 mg of **I** and **II**, respectively, in MeCN (3 mL), adding 326 mg of NH_2–X, stirring for a few hours, storing overnight at RT, filtering, washing with MeCN until the filtrate became colorless, and then drying in air until the weight remained constant. To prepare samples **3** and **4**, 323 mg of NH_2–X was dispersed in 2 mL of MeCN, then 5 and 30 μL of 8.2 M $HClO_4$ (1 and 6 eq of H^+ per Co-POM, respectively) were added followed by the addition of 157 mg of **II** dissolved in MeCN (1 mL). The mixtures were then stirred for a few hours, and the solid was filtered off, washed with MeCN, and dried in air. The percentages of Co-POM on the support were determined by both weight difference and elemental analysis.

2.1.5. The Co-POM/silica composite catalyst (sample *5*)

This material was prepared by a sol–gel method using **III** (10 wt%) and tetramethoxysilane. The molar ratio of reagents was as follows: Si:H_2O:MeOH:HCl = 1:12:9:0.0016. First, the silica precursor was hydrolyzed under acidic conditions at 50 °C for 1 h using 1/2 of the total amount of methanol and 2 mol of water (per 1 mol of Si). Subsequently, a solution composed of the remaining half of the methanol, the rest of water, and the Co-POM (10 wt%) was added to the first solution with vigorous stirring. After gelation and aging at room temperature, the resulting material was dried at 60 °C (2 days), ground, washed several times with water until the rinsing water was colorless, and dried.

2.2. Catalytic experiments and analyses of oxidation products

Catalytic oxidations were run in 15-mL thermostated glass vessels filled with air (1 atm). Catalytic IBA oxidation was carried out in MeCN at room temperature. Typically, freshly distilled IBA (0.4 mmol) was added to 1 mL of MeCN, containing a catalyst (0.002 mmol of Co), and the reaction mixture was vigorously stirred. The oxidation products were identified and quantified by GC (Tsvet-500, 30 m × 0.25 mm Supelco capillary column filled with MDN-5S, Ar, FID, internal standard—diphenyl).

Catalytic formaldehyde oxidation was carried out in H_2O at 20 and 40 °C. An aqueous solution (1–2 mL), containing

formaldehyde (0.23 M) and catalyst, was vigorously stirred and aliquots were taken and analyzed by both GC and titrimetric methods. The aldehyde conversion was not affected by the rate of stirring, indicating that the reaction is not limited by external mass transport. GC analyses of CH_2O and its oxidation products in liquid phase were performed using a Tsvet-500 gas chromatograph equipped with a 2 m × 3 mm steel column filled with Poropak-T (He, catharometer). The internal standard, ethanol, was added directly to an aliquot of the reaction mixture prior to GC measurements. Formaldehyde was also determined by a hydroxylamine method as described in [32], while formic acid was determined independently by titration with 0.05 M NaOH. The results of GC and titrimetric analyses coincided within 8–10%. The gas phase was analyzed using steel columns (2 m × 3 mm) filled with Poropak-T (98 °C) and Na–X (70 °C) for CO_2 and CO, respectively.

After the reactions, the catalysts were removed by filtration through a 0.45-μm filter, washed with MeCN (or H_2O), dried in air, and then reused. In some cases, the catalysts were washed with MeOH to remove adsorbed carbonic acid product or dried in vacuum.

2.3. Physical measurements

^{31}P NMR spectra were measured at room temperature on an MSL-400 Bruker NMR spectrometer at a frequency of 162 MHz, with a 50 kHz sweep width, 10 μs pulse width, and 0.2 s interpulse delay, relative to 85% H_3PO_4 as an external standard. FT-IR spectra were taken as 0.3 wt% samples in KBr pellets on a BOMEM-MB-102 spectrometer in the 250–4000 cm^{-1} range. Electronic absorption spectra of **I** and **II** were run on a Specord M40 spectrophotometer using 1-cm thermostated quartz cells. DRS-UV–vis measurements were performed on a Shimadsu UV–VIS 2501PC spectrophotometer. Cyclic voltammetric measurements were performed at 25 °C under argon using a BAS CV-50W voltammetric analyzer, a three-electrode cell, a glassy-carbon working electrode, a platinum auxiliary electrode, and an Ag/AgCl reference electrode (BAS). $TBAClO_4$ (0.1 M) was used as a supporting electrolyte. N_2 adsorption measurements were carried out using an ASAP-2400 Micromeritics instrument.

3. Results and discussion

3.1. Synthesis and characterization of Co-POMs

Cobalt(II)-monosubstituted Keggin POMs have been known since the late 1960s [10, and references therein]. The preparation of both $TBA_5PW_{11}CoO_{39}$ [22] and its protonated partner, $TBA_4HPW_{11}CoO_{39}$, [33] has been reported; however, the effect of protonation on the physicochemical and catalytic properties of Co-POMs has not been studied yet. We prepared both TBA-salts using slightly modified literature procedures [29,30] and characterized them by various physicochemical techniques. First, the presence of one acid proton per molecule of **I** was confirmed by potentiometric titration with methanolic TBAOH. A sharp breakpoint was observed upon addition of 1 eq of TBAOH to **I**. The IR spectra of solid **I** and **II** are very similar and display a fingerprint region that is characteristic of monosubstituted Keggin POMs (see Section 2). The IR spectra of **I** and **II** differ only in the range of 720–760 cm^{-1}. The bands in this range most likely can be attributed to Co–O–W vibrations [34], which are expected to be sensitive to protonation because M–O–W bridges in $XW_{11}M$ are sites of high nucleophilicity [40, and references therein]. UV–vis spectra of both **I** and **II** in MeCN solution are also very similar ($\lambda_{max} = 478$ and 480 nm with $\varepsilon = 167$ and 230 $M^{-1}\,cm^{-1}$, respectively) and very close to that of the sodium salt of $[PW_{11}CoO_{39}]^{5-}$, **III**, dissolved in 72% aqueous acetonitrile ($\lambda_{max} = 485$ nm [30]). Based on the results obtained in [30], we can suggest that the water molecule, which occupies the sixth coordination position of cobalt in the Co-POM, is replaced by an acetonitrile solvent molecule. Both MeCN and H_2O molecules can be removed from the cobalt coordination sphere by evacuation of **II**, which causes the color to change from pink to green. This is in agreement with the earlier finding of Katsoulis and Pope concerning interconversions of six-coordinate and five-coordinate Co(II) ions in Co-POMs [35]. Surprisingly, evacuation of **I** did not yield the green species.

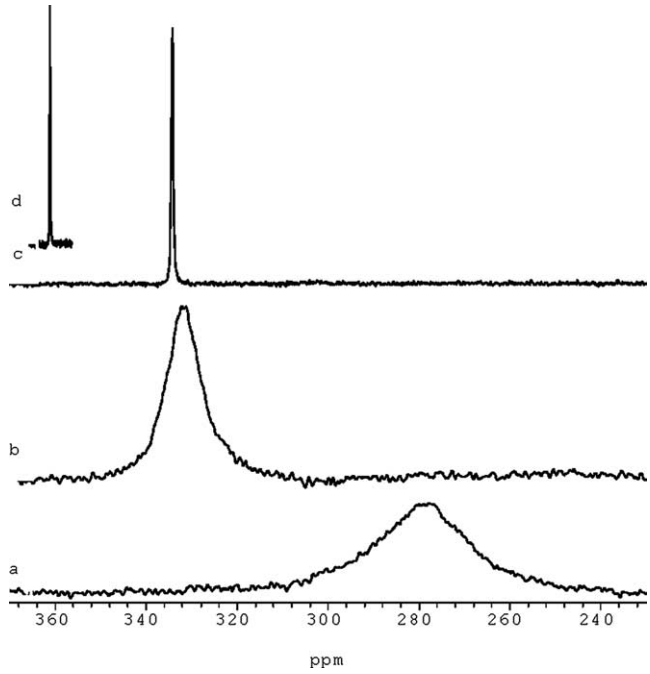

Fig. 1. ^{31}P NMR spectra of (a) $TBA_4HPW_{11}CoO_{39}$ (**I**), (b) $TBA_5PW_{11}CoO_{39}$ (**II**), (c) **I** after addition of 1 eq of TBAOH, and (d) $Na_5PW_{11}CoO_{39}$. The spectra were run at 20 °C, [Co-POM] = 0.05 M, in dry MeCN (a–c) and H_2O (d).

Contrary to the electronic and vibrational spectra of protonated **I** and nonprotonated **II**, the ^{31}P NMR spectra differ significantly (δ 279 and 335 ppm, respectively) (Figs. 1a and b). The signal of the protonated salt is broader

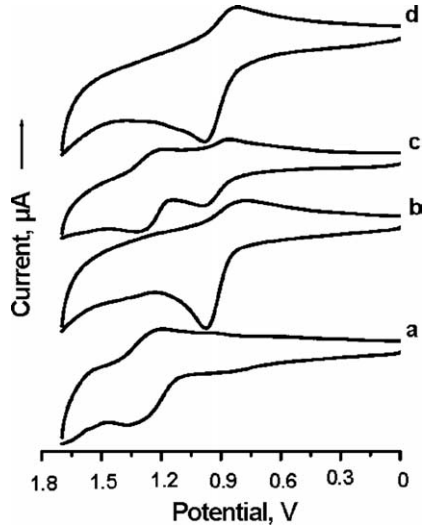

Fig. 2. Cyclic voltammograms of (a) **I**, (b) **(II)**, (c) **I** after addition of 0.25 eq of TBAOH, and (d) **I** after addition of 1 eq of TBAOH. Potentials are reported relative to a Ag/AgCl electrode. [Co-POM] = 0.001 M, scan rate, 100 mV/s, supporting electrolyte, 0.1 M $TBAClO_4$.

than that of the unprotonated one ($\nu = 3700$ and 1500 Hz, respectively), which is most likely due to slow proton mobility on the POM surface in dry MeCN [36–39]. The signal is significantly narrower (20 Hz) for $Na_5PW_{11}CoO_{39}$ in H_2O (Fig. 1d). Importantly, the signal at 279 ppm moves to 335 ppm upon addition of 1 eq of methanolic TBAOH to **I** (Fig. 1c). Simultaneously, the signal narrowing (up to 130 Hz) occurs, which is most likely due to formation of water during the reaction

$$TBA_4HPW_{11}CoO_{39} + TBAOH \rightleftharpoons TBA_5PW_{11}CoO_{39} + H_2O$$

as well as addition of MeOH (with TBAOH). Both H_2O and MeOH should increase the proton exchange rate. Indeed, signal narrowing and moving upfield occur upon addition of small amounts of water to a MeCN solution of **I**. Previously, we observed downfield and upfield shifts of the ^{31}P NMR signal upon protonation and deprotonation, respectively, of Ti-POMs in dry MeCN [38,40].

Protonated **I** and nonprotonated **II** show different electrochemical behavior (Fig. 2). A cyclic voltammogram of **I** performed at positive scan (0–1.7 V) showed the oxidation of Co(II) to Co(III) at $E_{1/2} = 1.26$ V ($E_{p,a} - E_{p,c} = 100$ mV) relative to Ag/AgCl (Fig. 2a). The cyclic voltammogram of **II** under the same conditions shows an analogous redox process at $E_{1/2} = 0.88$ V (Fig. 2b). Addition of 0.25 eq of TBAOH to **I** leads to a voltammogram in which the cobalt redox process has been split into two with $E_{1/2} = 1.26$ and 0.92 V (Fig. 2c). The observation of two distinct reduction peaks, one corresponding to the nonprotonated POM and one to the monoprotonated POM, is consistent with slow proton exchange between **I** and **II** on the CV time scale (100 mV/s). Complete neutralization of the acidic proton of **I** by the addition of 1 eq of TBAOH yields a voltammogram, in which a single cobalt redox peak is seen at $E_{1/2} = 0.89$ V (Fig. 2d), which is close to that of **II**. A similar shift in redox potential on protonation of $[SiW_{11}V^{IV}O_{39}]^{6-}$ has been observed and was ascribed to the increase of the anion charge upon deprotonation [37]. An increase in the redox potential upon protonation has been also documented for the Ti–peroxo complexes $[Bu_4N]_4[HPTi(O_2)W_{11}O_{39}]$ and $[Bu_4N]_5[PTi(O_2)W_{11}O_{39}]$ [40].

3.2. Supported Co-POMs

Transition-metal-substituted POMs can be attached to NH_2–silica by both dative bonding [22] and electrostatic bonding ($RNH_2 + H\text{-POM} = RNH_3{}^+POM^-$) [18,41]. In the latter case protons are needed to form $RNH_3{}^+$ groups. One of the aims of this work was to study the effect of protonation of the NH_2–silica on the catalytic and stability properties of the supported Co-POMs. For this purpose, samples of the supported POM catalysts, **1** and **2**, were obtained using **I** and **II**, respectively, while samples of the electrostatically supported POM catalysts, **3** and **4**, were prepared by the addition of 1 or 6 eq (per Co-POM) of $HClO_4$, respectively, to the mesoporous NH_2–xerogel followed by the addition of **II**. It is well known that POMs of the $XW_{11}M$ structure with M(II) and M(III), in contrast to many $XW_{11}M$ with M(IV) and M(V), are not stable in acid solutions and cannot be obtained as free acids [29,42,43]. Given this point, the acid should be added to the support before addition of the polyoxometalate. It was found that POMs partially decompose during the supporting process even in the absence of acid [22,44]. Specifically, it was found that the $[PW_{11}M]^{5-}$ structure is retained in the silica-supported M-POMs when TBA-salts of M-POMs (M = Co(II), Zn(II)) are added to NH_2-modified silica from a MeCN solution, while partial degradation of the M-POMs occurs when impregnation from an aqueous solution is employed even at neutral pH [22]. Taking this fact into account, we carried out immobilization of the Co-POMs only from acetonitrile using TBA-salts **I** and **II**.

Elemental analysis data for the supported Co-POMs are given in Table 1. The Co-POM loading is similar for samples **1** and **2** (13 and 11 wt%, respectively). At the same time, the

Table 1
Elemental analysis data for solid Co-POM catalysts

Sample	Co-POM[a]	Eq of H^+[b]	Co[c] (wt%)	Co-POM (wt%)	NH_2/Co-POM (mol/mol)
1	**I**	0	0.21 (0.08)	13	36
2	**II**	0	0.18 (0.04)	11	40
3	**II**	1	0.30	19	24
4	**II**	6	0.50 (0.34)	32	11
5	**III**	–	0.08 (0.08)	4	–

[a] Co-POM salt used for the preparation.
[b] The number of eq of $HClO_4$ (per Co-POM) added to NH_2–X.
[c] Weight percent of Co in the sample (the wt% of Co after three catalytic cycles of IBA oxidation inside parentheses; the reaction conditions are given in Table 3).

Table 2
Textural properties of solid Co-POM catalysts

Sample	S_{BET} (m^2/g)	V_p (cm^3/g)	d (nm)
$TBA_4HPW_{11}CoO_{39}$ (**I**)	2.5	0.01	–
NH_2–X	287	1.93	27
1	244	1.61	26
2	238	1.63	27
3	226	1.53	27
4	217	1.32	24
5	357 (442)[a]	0.17	1.5[b]

[a] Langmuir surface area.
[b] $d = 4V_p/S$ by Langmuir.

Co-POM loading increased with increasing amount of H^+ added initially to the support. Indeed, the lowest Co-POM loading (11 wt%) was obtained for sample **2** (no protons added), while the highest Co-POM loading (32 wt%) was found for sample **4**, in which 6 eq of $HClO_4$ (per Co-POM) was added to the NH_2–silica support prior to introduction of the POM. This can be readily rationalized if the high negative charge of Co-POM heteropolyanion, 5−, is taken into account. The more positively charged NH_3^+ groups in the support, the stronger the expected electrostatic binding of POM. Ideally, the binding process can be described by the following:

$$X\text{–}NH_2 + HClO_4 \rightleftharpoons X\text{–}NH_3^+ClO_4^-, \quad (1)$$

$$5X\text{–}NH_3^+ClO_4^- + TBA_5PW_{11}CoO_{39} \rightleftharpoons (X\text{–}NH_3^+)_5[PW_{11}CoO_{39}] + 5TBAClO_4. \quad (2)$$

In fact, after the addition of $HClO_4$ to NH_2–X in MeCN followed by filtration of the solid, the MeCN solution remained neutral, indicating that all protons were bound to the support. Importantly, in the absence of protons the process of anchoring **II** to NH_2–X is slower than the anion exchange in $X\text{–}NH_3^+ClO_4^-$ for $PW_{11}CoO_{39}^{5-}$. The latter proceeds almost immediately upon addition of **II**. This is not surprising given that in the former case a substitution of the coordinated H_2O (or MeCN) molecule for NH_2 ligand occurs in the primary coordination sphere of cobalt [22].

Textural properties of the initial NH_2–xerogel and supported Co-POMs are presented in Table 2. Both surface area and pore volume gradually decrease upon deposition of the Co-POMs. Pore-size distribution plots for NH_2–X and samples **1**–**4** are very similar (Fig. 3). Mesopores with a broad distribution of pore diameters around 27 nm are present. In contrast to NH_2-functionalized MCM-41 (mesopore diameter 3.0 nm) impregnated with Co-POM [22], an average pore diameter did not decrease upon introducing POM to NH_2–X and remained about 27 nm for samples **1**–**3**. Only when the Co-POM loading attained 32 wt%, did the average pore diameter reduce to 24 nm. Importantly, the textural properties do not suffer significantly even if the maximal amount of Co-POM is introduced. Indeed, the surface area of sample **4** is 76% of the surface area of the initial support (Table 2).

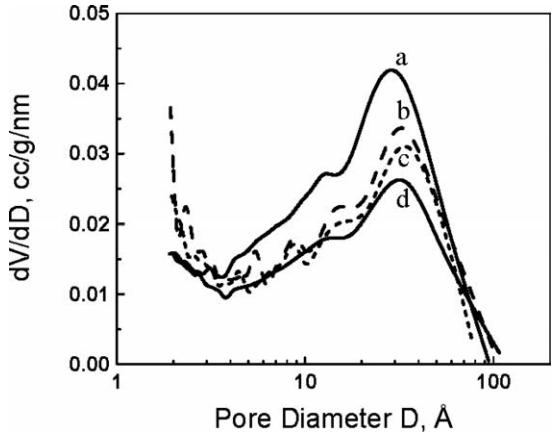

Fig. 3. Pore-size distribution plots from N_2 adsorption experiments: (a) X–NH_2, (b) sample **1**, (c) sample **3**, and (d) sample **4**.

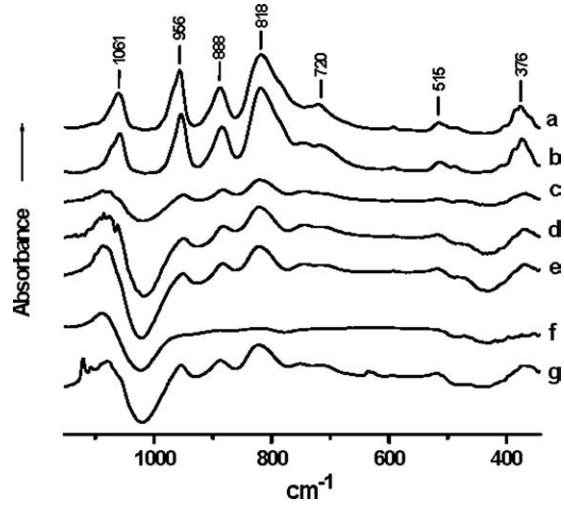

Fig. 4. FT-IR spectra of (a) **I**, (b) **II**, (c–e) samples **1**, **2**, and **4**, respectively, (f, g) samples **1** and **4**, respectively, after three catalytic cycles of IBA oxidation. In c–g the spectrum of the NH_2–xerogel was subtracted.

The FT-IR study was performed to assess whether the Co-POM structure is retained in the supported samples or not. The IR spectra of samples **1**–**4** are very similar after subtraction of the peaks due to NH_2–X (Fig. 4). The spectra are practically identical and clearly exhibit the principal stretching modes of the Keggin Co-POM unit (956, 888, 818, 752, 720 cm^{-1}) consistent with maintenance of the heteropolyanion structure after the supporting procedure. Unfortunately, the structure of the solid Co-POM-based materials could not be studied by ^{31}P solid-state MAS NMR because of the paramagnetic nature of cobalt(II).

DR-UV–vis spectroscopy was probed to characterize the cobalt center in the supported Co-POMs. DR-UV–vis spectra of the representative supported Co-POM samples, **1** and **3**, along with the spectrum of **I** are given in Fig. 5. The spectra of samples **1**, **3**, and **4** are very similar and resemble the spectrum of **III** in water, while the DR-UV–vis spectrum of **I** looks like a superposition of the spectra of $Na_5PW_{11}Co(H_2O)O_{39}$ and $Na_5PW_{11}Co(MeCN)O_{39}$ [30].

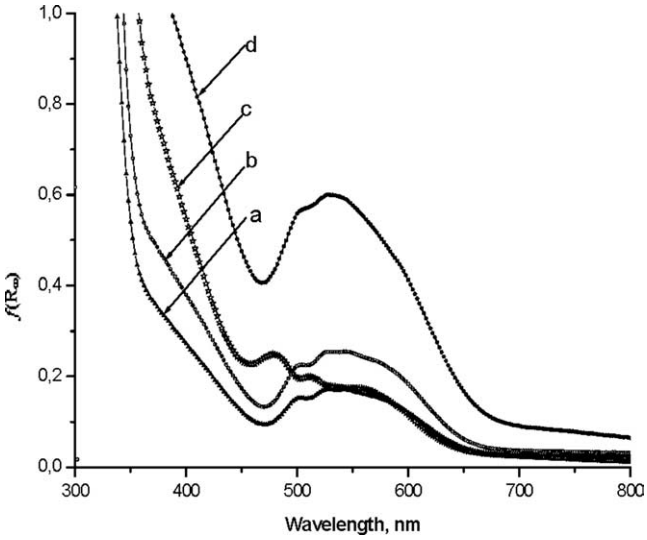

Fig. 5. DR-UV–vis spectra: (a, b) samples **1** and **3**, respectively, (c) **I**, and (d) Co-POM/silica composite material (sample **5**).

Table 3
Isobutyraldehyde (IBA) oxidation in the presence of Co-POM catalysts[a]

Run	Catalyst[b] (mg)	IBA conversion[c] (%)	IBAc yield[c,d] (%)	TOF_{av}[e] (h^{-1})
1	$TBA_4HPW_{11}CoO_{39}$ (**I**)	94	54	31
2	$TBA_5PW_{11}CoO_{39}$ (**II**)	71	40	24
3	–[f]	28	26	–
4	NH_2–X (60)	6	5	–
5	**1** (60)	92 (88, 77)	53 (52, 28)	31
6	**2** (66)	43 (37, 35)	35 (35, 28)	14
7	**3** (42)	52 (45, 50)	45 (22, 24)	17
8	**4** (25)	40	31	13
9	**5** (156)	91 (90, 93)	89 (85, 86)	30

[a] Reaction conditions: IBA, 0.4 mmol, Co complex, 0.002 mmol, air, 1 atm, MeCN, 1 mL, 20 °C, 6 h.
[b] For insoluble catalysts.
[c] Numbers in parentheses correspond to the second and third catalytic cycles.
[d] GC yield based on initial IBA.
[e] TOF_{av} = (moles of IBA consumed)/[(moles of Co) × 6 h].
[f] No catalyst present.

Importantly, the spectra of the Co-POM supported on the protonated NH_2–X differ from the spectra published for Co-POMs datively linked to NH_2–silica [22]. Indeed, no peaks or shoulders were observed in the range of 628–640 nm, indicating no formation of dative bonds between NH_2 groups and cobalt.

3.3. Co-POM/silica composite catalyst

Immobilization of heteropolyacids, $H_3PW_{12}O_{40}$ [17,45] and $H_3PMo_{12}O_{40}$ [45], within silica matrix has been successfully carried out. The introduction of lacunary POMs, XW_{11} [46], and a few POMs having $XW_{11}M$ structure [47,48] has also been published. Here we report the introduction of the Co-monosubstituted POM, **III**, into silica using a sol–gel procedure. Contrary to mesoporous samples **1**–**4**, the Co-POM/silica composite material (sample **5**) is microporous. Its textural properties (Table 2) are close to those obtained earlier for $H_3PW_{12}O_{40}$ [17,45] and $H_3PMo_{12}O_{40}$ [45]. The DR-UV–vis spectrum of **5** is very similar to that of Co-POM supported on the protonated NH_2–X (Fig. 5) and that of **III** in aqueous solution [30].

3.4. Aerobic oxidation of isobutyraldehyde

The catalytic activity of the solid Co-POMs for the aerobic oxidation of IBA was evaluated and compared with the catalytic properties of the homogeneous Co-POMs (**I** and **II**). The results are presented in Table 3. Interestingly, the IBA conversion in the absence of any catalyst is 28% (run 3), while in the presence of the support (NH_2–X) the conversion is just 6% (run 4), thus indicating that the support acts as an inhibitor for the IBA oxidation. In the presence of all solid Co-POM catalysts the oxidation of IBA readily proceeds in MeCN at room temperature to yield isobutyric acid (IBAc) as the main oxidation product. The best results were obtained for the Co-POM/silica composite material (sample **5**, run 9). The selectivity toward IBAc was fairly high and attained 98% at 90–93% IBA conversion after 6 h, with an average turnover frequency (TOF_{av}) of 30 h^{-1}. The activity (in terms of TOF_{av}) of supported sample **1** (run 5) was comparable with that of sample **5**; however, the IBAc yield was significantly lower (53% versus 89% for sample **5**). The activity of sample **2**, prepared from protonless **II**, was lower than the activity of sample **1** prepared from **I** containing 1 proton per POM molecule (compare runs 5 and 6). The addition of 1 eq of H^+ to NH_2–X before adding **II** (sample **3**) resulted in the increase of both Co-POM loading (Table 1) and the catalyst activity (Table 3, runs 6 and 7). Meanwhile, the level of the activity of sample **1** was not attained and further addition of H^+ not only resulted in increasing Co-POM loading but also led to reductions in both IBA conversion and IBAc yield. This decrease in activity may result from decreasing mesopore diameter and volume (Table 2); moreover, Co-POM at high concentrations (loading) may act as an inhibitor rather than a catalyst via capturing active acylperoxy radicals [24–26].

Interestingly, the catalytic activity of **I** is higher than that of **II** (94 and 71% of IBA conversion, respectively), indicating that the presence of proton is important for the activity of Co-POMs in the IBA oxidation. This may be due to higher redox potential of cobalt in **I** compared to **II** (Fig. 2). Note that, in general, the rate of the IBA oxidation is slower than the rate of its oxidation in the presence of a conjugated organic substrate, e.g., alkene [24]. What is significant is that the activity of the best solid Co-POM catalysts (samples **1** and **5**) is the same as the activity of homogeneous **I** (TOF values of 30 and 31; Table 3). The selectivity to IBAc is similar for sample **1** and parent **I** (57%), while for sample **5** it reaches 98%.

Inhibition of the Co-POM-catalyzed IBA oxidation by the reaction product, IBAc, evidently takes place (Fig. 6).

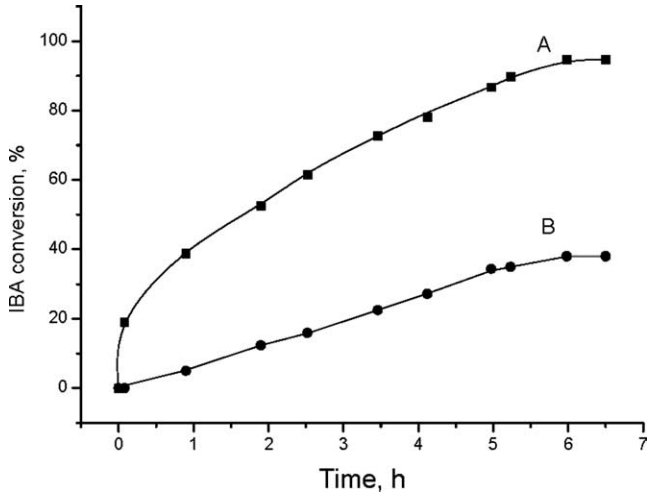

Fig. 6. IBA consumption vs time in the presence of **I**: without additives (curve A) and with 0.1 M IBAc added at the beginning of the reaction (curve B). For reaction conditions, see Table 3.

We studied the interaction of **II** with IBAc in MeCN using both UV-vis and ^{31}P NMR. The addition of the carboxylic acid resulted in alteration of both spectra. These changes are consistent with the replacement of a terminal acetonitrile ligand on cobalt with a carboxylate ligand.

$$TBA_5PW_{11}Co(MeCN)O_{39} + (CH_3)_2CHCOOH \rightleftharpoons TBA_5HPW_{11}Co(OOCCH(CH_3)_2)O_{39} + MeCN. \quad (3)$$

The monotonic upfield progression of the Co-POM ^{31}P NMR chemical shift with increasing IBAc concentration strongly suggests the formation of a 1:1 complex between Co-POM and IBAc (**II**–IBAc) with exchange between **II** and **II**–IBAc being rapid on the ^{31}P NMR time scale [49]. The constant for Eq. (3), $K_3/[MeCN] = [\mathbf{II}\text{–IBAc}]/([\mathbf{II}]\times[IBAc])$ was assessed from Eq. (4) (Fig. 7) as described in [49,50]. The value of 140 M^{-1} was found.

$$\frac{1}{\delta_{obs} - \delta_a} = \frac{1}{\Delta} + \frac{1}{K\Delta}\frac{1}{[IBAc]_0}, \quad (4)$$

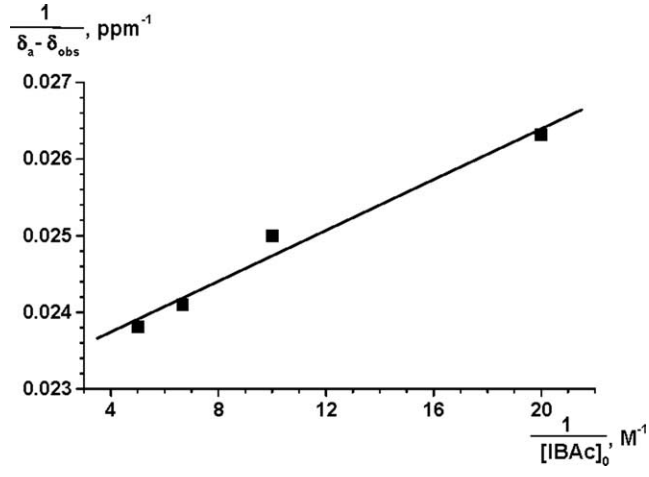

Fig. 7. Plot of $1/(\delta_a - \delta_{obs})$ versus $1/[IBAc]_0$ for interaction of **II** with IBAc.

where δ_{obs} is the observed ^{31}P NMR chemical shift of **II**–IBAc, δ_a is the chemical shift of **II** in the absence of IBAc, and $\Delta = \delta_b - \delta_a$ (δ_b is chemical shift of the individual complex **II**–IBAc that could be observed if concentration of IBAc tended to infinity).

The superior catalytic properties of sample **5** in the IBA oxidation are likely due to its microporous structure, that may minimize catalyst deactivation by the IBAc product (decreased diffusion and penetration of the IBAc molecules to the active Co centers).

3.5. Aerobic oxidation of formaldehyde

Oxidation of CH_2O in the presence of Co-POMs was carried out in water at 20 and 40 °C. The results are presented in Table 4. Not surprisingly, the CH_2O conversions are generally lower than those observed in the IBA oxidations. The aerobic oxidation (air only) of CH_2O under mild conditions is quite challenging because formaldehyde is far harder to oxidize, either by autoxidation (radical-chain reductant-free O_2-based oxidation) or by other oxidation processes, than nearly all aldehydes and ketones [3]. As in the case of IBA oxidation, the catalytic activity of homogeneous **III** did not exceed the activities of the solid Co-POM catalysts. Interestingly, **I**, which is insoluble in water, gave results which are close to those of soluble **III**. The CH_2O conversion increased with decreasing pH (Table 4). Formic acid was the only oxi-

Table 4
CH_2O oxidation in the presence of Co-POM catalysts[a]

Catalyst	T (°C)	CH_2O conversion[b] (%)	HCOOH yield[b,c] (%)
$Na_5PW_{11}CoO_{39}$[d] (**III**)	40	19[e]	9[e]
$TBA_5PW_{11}CoO_{39}$ (**II**)	40	12	3
$TBA_4HPW_{11}CoO_{39}$ (**I**)	40	20 (11)	5 (4)
–[f]	40	0	0
NH_2–X	20	38	0
NH_2–X	40	69[g] (0)	0
1	20	41	2
1	40	40 (22)	3 (3)
2	20	33	0
2	40	33	0
3	20	29	0
3	40	39 (20)	5 (3)
4	20	35	3
4	40	51	8
5[h]	40	13 (10)	3 (2)

[a] Reaction conditions: CH_2O, 0.23 M; catalyst, 100 mg; air, 1 atm; H_2O, 1 mL; pH 2.7; 5 h.
[b] Numbers in parentheses correspond to the second catalytic run.
[c] GC yield based on initial CH_2O.
[d] 6 mM.
[e] When the reaction was run at pH 6.4, CH_2O conversion and HCOOH yield were lower (11 and 6%, respectively).
[f] No catalyst present.
[g] Chemisorption of CH_2O and its oxidation products is very likely occurring.
[h] Reaction at pH 6.4; when the reaction was run at pH 2.7, CH_2O conversion and HCOOH yield were 20 and 6%, respectively.

dation product detectable in the liquid phase for the reactions with **III** and **I**; however, the selectivity was rather low compared to the recently discovered Ce-POM catalyst [51]. Although the concentration of CH_2O decreased considerably in the presence of the supported Co-POM catalysts, the collective yield of CH_2O oxidation products detected by GC in either the liquid or the gas phase was low. This is most likely a result of adsorption of formaldehyde and formic acid (and probably CO and CO_2 also) on the NH_2–X support. Similar data obtained at 20 and 40 °C for samples **1** and **2** support this suggestion. The highest decrease of CH_2O concentration in water was observed in the presence of NH_2–X alone, which doubtless reflects the chemisorption of formaldehyde on the porous material. Indeed, this material does not work repeatedly (line 6, Table 4). Significantly, the activity of the Co-POM/SiO_2 composite material was close to the activity of homogeneous **III** and heterogeneous **I** under comparable pH conditions.

3.6. Catalyst recycling

No loss of the catalytic activity was observed after at least 3 catalytic cycles of the IBA oxidation when the Co-POM/silica composite (sample **5**) was used as the catalyst (Table 3). Indeed, elemental analysis confirmed no loss of cobalt in sample **5** after 3 catalytic runs (Table 1). This stability to leaching is likely due, in part, to the microporous structure of the composite material (see Table 2). The situation is worse in the case of Co-POMs supported on NH_2–X. Sample **1** gave similar results after two catalytic runs; however, some loss in activity was observed in the third run. Our attempts to reactivate the sample by washing with MeOH or evacuation at reduced pressure were unsuccessful, indicating that at least some changes in this catalyst were irreversible. Moreover, both FT-IR (Fig. 4f) and elemental analysis data (Table 1) showed that a substantial loss of Co-POM occurred from the solid matrix. The stability of the supported Co-POMs increases with increasing amount of acid added initially to NH_2–X (compare Figs. 4f and 4g). However, despite the fact that IBA conversion remained quite constant for three successive catalytic runs of sample **3**, the IBAc yield gradually decreased. Recycling of the solid Co-POM catalysts used in CH_2O oxidation in water is also problematic because some porous silicas are known to exhibit instability when exposed to water [52]. One can see from the data in Table 4 that, in contrast to the IBA oxidation, some loss of the activity occurs even in the case of the use of the microporous Co-POM/silica composite catalyst.

4. Conclusions

The present study revealed that two different TBA salts of $[PW_{11}CoO_{39}]^{5-}$, **I** (TBA_4H) and **II** (TBA_5), can be obtained depending on the acidity. These two salts show predictably different ^{31}P NMR and electrochemical characteristics in MeCN. The protonated salt **I** has a higher redox potential and shows higher catalytic activity in the aerobic IBA oxidation at room temperature than the nonprotonated **II** does. Both **I** and **II** can be anchored to NH_2-modified mesoporous silica. Both IR and DR-UV–vis studies confirm retention of the Keggin structure of the Co-POM in the resulting solid materials. The supported **I** shows better catalytic properties than the supported **II** (IBA conversion after 6 h was 92 and 43%, respectively). The catalytic activity of **I** supported on NH_2–silica is as high as the activity of homogeneous **I** (TOF = 31 h^{-1}); however, some loss of catalytic activity is observed after three catalytic cycles due to Co-POM leaching during the oxidation process. This leaching has been confirmed by both IR and elemental analysis data. The preliminary addition of an acid to NH_2–silica produces $NH_3^+X^-$–silica and facilitates the introduction of Co-POM to the support via ion exchange with retention of the Co-POM structure. The more acid that is added to the support, the higher the Co-POM loading, and the more stable the catalyst. However, the increase of the Co-POM loading leads to reduced catalytic activity.

A Co-POM ($Na_5PW_{11}CoO_{39}$, **III**) was immobilized in silica matrix using a sol–gel procedure. DR-UV–vis measurements confirmed preservation of the Co-POM structure in the resulting microporous Co-POM/silica composite materials. This material shows high activity and selectivity in the aerobic oxidation of IBA (conversion 90–93%, selectivity to IBAc 98% after 6 h at room temperature) and, in contrast to the Co-POMs supported on NH_2–silica, this sol–gel-incapsulated Co-POM heterogeneous catalyst can be used repeatedly without suffering a loss in catalytic activity and selectivity.

Both the Co-POMs supported on NH_2–silica and the Co-POM/silica composite materials were tested as catalysts for the aerobic oxidation of formaldehyde in water. The activity of the composite material is close to the activity of homogeneous **III** and heterogeneous **I**. However, in contrast to the IBA oxidation, some loss in activity occurs after recycling. The activity of the Co-POMs supported on the NH_2–silica in this reaction is most likely due to chemisorption of CH_2O on these materials.

Acknowledgments

CRDF (Grant RC1-2371-NO-02) funded the research. We thank T.A. Larina and K.F. Obzherina for DR-UV–vis and IR measurements. We also thank G.M. Maksimov and N.N. Trukhan for preliminary syntheses and other help.

References

[1] R.A. Sheldon, J.K. Kochi, Metal-Catalyzed Oxidations of Organic Compounds, Academic Press, New York, 1981.
[2] S.A. Maslov, E.A. Blumberg, Russ. Chem. Rev. 45 (1976) 303.

[3] R.M. Harrison, in: R.E. Hester, R.M. Harrison (Eds.), Indoor Air Pollution and Health, vol. 10, Royal Society of Chemistry, Cambridge, 1996, p. 101.
[4] R.A. Sheldon, J. Dakka, Catal. Today 19 (1994) 215.
[5] G. Centi, M. Misono, Catal. Today 41 (1998) 287.
[6] R.A. Sheldon, R.S. Downing, Appl. Catal. A 189 (1999) 163.
[7] J.S. Rafelt, J.H. Clark, Catal. Today 57 (2000) 33.
[8] W.F. Hoelderich, Catal. Today 62 (2000) 115.
[9] J.H. Clark, C.N. Rhodes, Clean Synthesis Using Porous Inorganic Solid Catalysts and Supported Reagents, Royal Society of Chemistry, Cambridge, UK, 2000.
[10] M.T. Pope, Heteropoly and Isopoly Oxometalates, Springer, Berlin, 1983.
[11] J.B. Moffat, Metal–Oxygen Clusters: The Surface and Catalytic Properties of Heteropoly Oxometalates, Kluwer/Plenum, New York, 2001.
[12] J.J. Borras-Almenar, E. Coronado, A. Müller, M.T. Pope, in: Polyoxometalate Molecular Science, Kluwer, Dordrecht, 2003.
[13] C.L. Hill, C.M. Prosser-McCartha, Coord. Chem. Rev. 143 (1995) 407.
[14] N. Mizuno, M. Misono, Chem. Rev. 98 (1998) 199.
[15] R. Neumann, Prog. Inorg. Chem. 47 (1998) 317.
[16] C.L. Hill, in: A.G. Wedd (Ed.), Comprehensive Coordination Chemistry II, vol. 4, Elsevier Science, New York, 2004, p. 679.
[17] Y. Izumi, Res. Chem. Intermed. 24 (1998) 461.
[18] A.M. Khenkin, R. Neumann, A.B. Sorokin, A. Tuel, Catal. Lett. 63 (1999) 189.
[19] L. Xu, E. Boring, C.L. Hill, J. Catal. 195 (2000) 394.
[20] A.N. Kharat, P. Pendleton, A. Badalyan, M. Abedini, M.M. Amini, J. Mol. Catal. A: Chem. 175 (2001) 277.
[21] W. Kaleta, K. Nowinska, Chem. Commun. (2001) 535.
[22] B.J.S. Johnson, A. Stein, Inorg. Chem. 40 (2001) 801.
[23] N. Mizuno, T. Hirose, M. Tateishi, M. Iwamoto, Chem. Lett. (1993) 1839.
[24] O.A. Kholdeeva, V.A. Grigoriev, G.M. Maksimov, M.A. Fedotov, A.V. Golovin, K.I. Zamaraev, J. Mol. Catal. A: Chem. 114 (1996) 123.
[25] O.A. Kholdeeva, V.N. Romannikov, A.V. Tkachev, I.V. Khavrutskii, K.I. Zamaraev, Stud. Surf. Sci. Catal. 108 (1997) 337.
[26] O.A. Kholdeeva, I.V. Khavrutskii, V.N. Romannikov, A.V. Tkachev, K.I. Zamaraev, Stud. Surf. Sci. Catal. 110 (1997) 947.
[27] R. Giannandrea, P. Mastrorilli, C.F. Nobile, G.P. Suranna, J. Mol. Catal. 94 (1994) 27.
[28] G. Kowalski, J. Pieichowski, M. Jasieniak, Appl. Catal. A 247 (2003) 295.
[29] T.J.R. Weakley, S.A. Malik, J. Inorg. Nucl. Chem. 29 (1967) 2935.
[30] T.J.R. Weakley, J. Chem. Soc., Dalton Trans. (1973) 341.
[31] C. Alie, R. Pirard, A.J. Lecloux, J.-P. Pirard, J. Non-Cryst. Solid. 246 (1999) 216.
[32] J.F. Walker, Formaldehyde, third ed., Reinhold, New York, 1964.
[33] C.L. Hill, R.B. Brown, J. Am. Chem. Soc. 108 (1986) 536.
[34] G.M. Maksimov, G.N. Kustova, K.I. Matveev, T.P. Lazarenko, Koord. Khim. 15 (1989) 788 (in Russian).
[35] D.E. Katsoulis, M.T. Pope, J. Am. Chem. Soc. 106 (1984) 2737.
[36] R.G. Finke, B. Rapko, R.J. Saxton, P.J. Domaille, J. Am. Chem. Soc. 108 (1986) 2947.
[37] S.P. Harmalker, M.T. Pope, J. Inorg. Biochem. 28 (1986) 85.
[38] O.A. Kholdeeva, G.M. Maksimov, R.I. Maksimovskaya, L.A. Kovaleva, M.A. Fedotov, V.A. Grigoriev, C.L. Hill, Inorg. Chem. 39 (2000) 3828.
[39] Y. Hou, C.L. Hill, J. Am. Chem. Soc. 115 (1993) 11823.
[40] O.A. Kholdeeva, T.A. Trubitsina, R.I. Maksimovskaya, A.V. Golovin, W.A. Neiwert, B.A. Kolesov, X. López, J.-M. Poblet, Inorg. Chem. 43 (2004) 2284.
[41] W. Kaleta, K. Nowinska, Chem. Commun. (2001) 535.
[42] G.M. Maksimov, R.I. Maksimovskaya, I.V. Kozhevnikov, Zh. Neorgan. Khim. 37 (1992) 2279.
[43] G.M. Maksimov, Russ. Chem. Rev. 64 (1995) 480.
[44] A. Sinnema, R.J.J. Jansen, K. Pamin, H. van Bekkum, Catal. Lett. 30 (1995) 241.
[45] J. Mrowiec-Bialon, W. Turek, A.B. Jarzebski, React. Kinet. Catal. Lett. 76 (2002) 213.
[46] Y. Guo, Y. Yang, C. Hu, C. Guo, E. Wang, Y. Zou, S. Feng, J. Mater. Chem. 12 (2002) 3046.
[47] Q. Wu, Mater. Lett. 56 (2002) 19.
[48] Q. Wu, Mater. Chem. Phys. 77 (2002) 204.
[49] K. Zamaraev, New J. Chem. 18 (1994) 3.
[50] K.P. Bryliakov, E.P. Talsi, S.N. Stas'ko, O.A. Kholdeeva, S.A. Popov, A.V. Tkachev, J. Mol. Catal. A: Chem. 194 (2003) 79.
[51] O.A. Kholdeeva, M.N. Timofeeva, G.M. Maksimov, R.I. Maksimovskaya, W.A. Neiwert, C.L. Hill, submitted.
[52] R.K. Iler, The Chemistry of Silica, vol. 1, Wiley, New York, 1979.